Dissecting The Salinity-Dependence Of Wettability In Oil/Brine/Calcite System Using Molecular Simulations

Mohamed S. Al-Hosani, Arjun Valiya Parambathu, Fernando M. Yrazu, D. Asthagiri, and Walter G. Chapman*

Department of Chemical and Biomolecular Engineering, Rice University, 6100 Main St., Houston, Texas 77005, USA

E-mail: wgchap@rice.edu

Abstract

Low salinity water flooding has shown great promise due to its cost-effectiveness and low environmental impact for improving and sustaining oil production. It is believed that injecting water with ionic strength lower than that of the reservoir changes the reservoir from less to more water-wet and enhances oil recovery. This alteration phenomenon is not well understood, due to complex interactions between oil, water, and rock. Here we use molecular simulations to characterize the wettability of the $10\bar{1}4$-face of calcite in a calcite/brine/oil system, and address how wettability is altered by changing ionic strength and salt type (NaCl vs. $CaCl_2$). Using the test area method we calculate the superficial tension of the fluids against the solid and the surface tension between the two fluid phases. As the salinity is decreased, the wetting of calcite by brine is progressively less favored, contrary to what might be expected based on low salinity flooding. However, as salinity is decreased, forming the oil-brine interface is more favored. On balance, it is the latter effect that leads to the enhanced wetting of calcite by brine in the oil-brine-calcite system, and it is suggested as an important element in the physics underlying low-salinity flooding.

Introduction

Exploration and geological investigations carried out by the oil and gas industry have shown that a majority of the oil reserves, particularly heavy crude which accounts for up to 70% of global petroleum resources, is trapped in underground reservoirs due to high capillary forces and narrow pores.[1] Unlocking only 1% of these trapped reserves would potentially produce an additional 88 billion barrels of oil, equivalent to several years of oil production at the current rate.[2] Such a large increase in oil production would be significant not only in terms of meeting global energy needs, but also in terms of the profitability and sustainability of the oil and gas industry. However, studies and practical operations in oil fields have shown that these trapped reserves cannot be recovered using conventional primary or secondary techniques.[3] To further increase recovery, a tertiary method, also known as enhanced oil recovery (EOR), is used. There are several different EOR approaches including thermal injection,[4] chemical injection,[5] gas injection,[6] and low-salinity water flooding (LSWF).[7] Among these methods, LSWF has been recognized as a promising, low-cost method to enhance oil recovery. The history, application, economical feasibility, laboratory and field observations, working conditions and proposed mechanisms of low salinity flooding have been investigated, for example, in refs. 8–14.

In LSWF, altering the wettability of calcium carbonate rocks from oil-wet to water-wet has been accepted as a dominant aspect in the enhancement of oil recovery. However, the driving forces for such a wettability alteration are still not fully understood, mainly because of the complex nature of the interactions between oil, water, and mineral surface. Indeed, several seemingly contradictory mechanisms and hypotheses have been proposed in the literature.[15,16] At a fundamental level, a molecular scale understanding of why low salinity flooding works and its dependence on reservoir type, including oil constituents and brine composition, remains elusive. In a step towards seeking this fundamental understanding, here we explore the response of the wettability of calcite effected by changes in the ionic strength of brine.

At equilibrium, wetting depends on the interfacial forces that exist between the fluids on the one hand and the fluids and the solid on the other. The contact angle (Fig. 1) is a
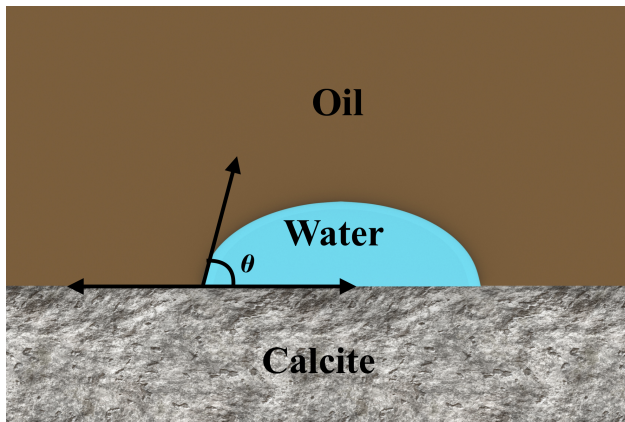

Figure 1: Schematic of oil/brine/calcite contact angle.

convenient parameter characterizing the preferential wetting of the solid by one or the other fluid phase. A contact angle of 0° indicates that the calcite surface is completely water-wet, whereas a value of 180° indicates that it is completely oil-wet. When both liquids tend to wet the surface about equally, i.e., $\theta \approx 90^o$, the system is said to be neutral-wet.[17,18]

Measuring contact angles experimentally is a challenging problem. Conceptually, the contact angle can be obtained by imaging the interfacial profile of a sessile oil drop in contact with a calcite surface in the presence of brine. However, there are several challenges. Firstly, sufficient care needs to be undertaken to ensure that the fluids and calcite are well equilibrated. Secondly, attention needs to be paid in preparing the calcite surface: the desired goal of an atomically smooth surface is almost never realized in practice. Thirdly, sufficient care needs to be exercised in preventing unwanted surface reactions. Finally, replicating reservoir conditions of high temperature and pressure proves rather difficult.

Our aim here is to use computer simulations to complement and enhance the interpretation of experimental results. In a computer simulation, we can investigate various scenarios (such as having an ideal crystal surface or extreme conditions) which are otherwise inaccessible in the laboratory, thereby allowing us to dissect the factors that influence the wettability

of the mineral surface. To this end, here we study the wettability of calcite under ambient conditions and investigate the molecular-scale physics of how solvent composition governs low-salinity flooding.

The rest of the paper is organized as follows. In section 2, we briefly sketch the theory and in section 3, we present the simulation models and methodology. The results are collected in section 4, followed by conclusions in section 5.

Theory

The thermodynamics of fluids in contact with solid surfaces has engendered much debate, including over the meaning of quantities such as the "surface" tension in the context of solid-fluid interface.[19–21] (In contrast to a liquid, it is not conceivable to strain the surface of the solid without simultaneously straining the bulk.) However, these debates are avoided by simply following Gibbs'[22] development. (See also Ref. 23.) To this end, let

$$\sigma = \left(\frac{\partial F}{\partial \Omega}\right)_{T,V,n_i}.$$

(1)

Here F is the Helmholtz free energy of the system, where the system comprises two homogeneous phases (either two fluid phases or a fluid in contact with a solid) separated by the interface; Ω is the surface area of the interface, V is the total volume of the system, and n_i denote the moles of component i. For two liquids separated by an interface, Eq. 1 is precisely the interfacial tension. Using Eq. 1, for a solid(s)-liquid(l) interface, we have σ_{sl}, and for a solid(s)-vacuum(v) interface, we have σ_{sv}. On this basis, following Gibbs, we define

$$\zeta_{sl} = \sigma_{sl} - \sigma_{sv}$$

(2)

as the "superficial" tension (or surface tension) of the liquid in contact with the solid. For an inelastic solid, we then have Young's equation

$$\sigma_{ow} \cdot \cos(\theta) = \zeta_{so} - \zeta_{sw} \tag{3}$$

where ζ_{so} or ζ_{sw} is the superficial (surface) tension of the respective fluid phase against the solid and σ_{ow} is the oil-water interfacial tension. We will use Eq. 3 to characterize the oil/brine/calcite contact.

From the thermodynamic definition (Eq. 1), we can approximate σ as

$$
\begin{aligned}
\sigma = \left(\frac{\partial F}{\partial \Omega}\right)_{T,V,N_i} &\approx \left(\frac{[F(\Omega_0 + \Delta\Omega) - F(\Omega_0)] - [F(\Omega_0 - \Delta\Omega) - F(\Omega_0)]}{2\Delta\Omega}\right) \\
&\equiv \left(\frac{F^+(\Delta\Omega) - F^-(\Delta\Omega)}{2\Delta\Omega}\right)
\end{aligned} \tag{4}
$$

In the canonical ensemble, $F^{\pm}(\Delta\Omega) = -k_{\mathrm{B}}T \ln \langle \exp(-\Delta U^{\pm}/k_{\mathrm{B}}T)\rangle_0$, where $\Delta U^{\pm}$ is the change in the potential energy of the system for the change in interfacial area ($\Delta\Omega$) and the averaging ($\langle \ldots \rangle_0$) is over the reference, denoted by subscript '0'. Thus, we find

$$\sigma \approx \frac{-k_{\mathrm{B}}T}{2\Delta\Omega} \left(\ln \langle \exp(-\Delta U^+/k_{\mathrm{B}}T)\rangle_0 - \ln \langle \exp(-\Delta U^-/k_{\mathrm{B}}T)\rangle_0 \right) . \tag{5}$$

Eq. 5 is the basis for the test area simulation method (TASM).[24] Please note that for a liquid in contact with a solid, Eq. 5 straightforwardly gives the surface tension defined in Eq. 2.

TASM has been used satisfactorily in the context of liquid-vapor, liquid-liquid, and solid-liquid interfaces; for example, see refs. 25–28. Nevertheless, as has been emphasized before,[29] Eq. 5 has the same limitations as any single-stage perturbative approach[30,31] and thus care is required in its use. In this work, the relative area change, $|\Delta\Omega/\Omega_0| \approx 10^{-4}$ (see below), ensures that the energy perturbations are small, on average about 0.5 $k_{\mathrm{B}}T$. Past experience with free energy perturbation and exploratory calculations on water confirms that this level of perturbation ensures that the free energy change in the forward direction ($\Omega_0 \to \Omega_0 \pm \Delta\Omega$)

6

is consistent with the corresponding change in the reverse direction $(\Omega_0 \pm \Delta\Omega \to \Omega_0)$.

In the earliest use of area perturbation that we are aware of, instead of Eq. 5 Salomons and Mareschal[32] have used Bennett's approach to obtain the free energy change in perturbing the area. Not surprisingly they are able to use a larger area perturbation than what Gloor et al.[24] had to use for the Lennard-Jones fluid, emphasizing the need for care noted above. For the solid-liquid interfaces studied here, we note that area perturbation is about a factor of 5 smaller than what Vega and de Miguel[25] used in their studies on water.

Robust and efficient alternatives to area sampling do exist. These include, for example, the approach by Guo and Errington[33] who use grand canonical Monte Carlo simulations to calculate the free energy change in growing one fluid layer next to the solid in the presence of the other liquid, or variations of the cleaving wall idea, for example see refs.,[34–36] where the free energy to create an interface is directly obtained from simulations. While using one of these alternatives is to be preferred, especially in the context of complex fluid mixtures that are of interest in studies on wettability in the oil and gas industry, in this study we have chosen to work with Eq. 5 for simplicity.

Simulation Methodology

The amorphous builder provided with the MedeA® software[37] was used to build all the required systems. The PCFF+ force field[38] (an extension of PCFF[39]) within MedeA® was used to define the inter-molecular interactions. This force field is capable of adequately describing the thermodynamic properties of organic compounds and water. The Waldman-Hagler[40] sixth-power mixing rule was used for Lennard-Jones (LJ) interactions between unlike species.

The initial system to compute the liquid/liquid interfacial tension was created by placing a box containing 6900 water molecules against a box containing an approximately 85:15 (% wt) mixture of dodecane and toluene, which is our model for the oil (i.e., 575 dodecane and

184 toluene molecules.) The dimensions of each box were 4.0 nm × 10.4 nm × 5.0 nm in the x, y, and z directions, respectively. The different combinations of ionic strength and salt type of the aqueous phase are shown in Table 1.

Table 1: Ionic strengths and composition (in number of ions) of the various aqueous phases simulated in this work. The salts are NaCl and CaCl$_2$. The number of Cl$^-$ ions is set by electroneutrality.

Ionic Strength (M)	Na$^+$	Ca^{2+}
0.15	18	6
0.53	66	22
1.09	136	45
3.16	391	131
4.98	615	206

To create the liquid/solid interface, we first built the calcite crystal using 6 atomic layers (total dimensions 4.0 nm × 10.4 nm × 17.3 nm). The z direction is normal to the $10\bar{1}4$ face of the crystal. (The $10\bar{1}4$ face has been used in several studies[41–43] and is considered to be a good choice on account of its thermodynamic stability.[44–47]) The liquid (oil or brine) slab, of dimensions noted above, was then placed between two calcite slabs.

All simulations were performed at 298.15 K and 1 atm using the LAMMPS[48,49] code integrated within the MedeA$^®$ software environment.[37] We use a 1 fs time step to integrate the equations of motion. The temperature and pressure were controlled using a Nosé-Hoover thermostat[50] and a Nosé/Hoover barostat,[51] respectively. Periodic boundary conditions were applied in all three directions. Long-ranged electrostatic interactions were handled using the particle-particle-particle-mesh (PPPM) method, with forces converged to a relative error of $1 \cdot 10^{-5}$. The energy of the initial system was minimized using the conjugate gradient approach for 30000 steps. After energy minimization, the system was equilibrated in two stages: (i) over 2.5 ns in the NpT ensemble, and (ii) for an additional 0.5 ns in the NVT ensemble. Following these equilibration steps, the subsequent production run of 20 ns was carried out in the NVT ensemble and frames saved every 0.5 ps. For the saved configurations, the system was perturbed in the x and y directions by $|\delta x| \approx |\delta y| \approx 0.635$Å which changed the

interfacial area ($\delta\Omega$) by $\approx 0.4\text{Å}^2$; $|\delta z|$ was adjusted accordingly to keep the volume constant.

Results and Discussions

The test area method predicts a value of $\sigma_{wv} = 64 \pm 2$ (2σ) mN/m for the PCFF+ water model used in this study. This value can be compared with the 68 ± 2 (2σ) mN/m obtained using the stress tensor. These results are also in fair agreement with the experimental value of 72 mN/m at 298 K.[52–54] Likewise $\sigma_{ov} = 21 \pm 2$ (2σ) mN/m using TASM agrees well with 20 ± 2 (2σ) mN/m obtained using the pressure tensor method.

For the bare calcite surface, using the TASM we find $\sigma_{sv} = 579 \pm 5$ mN/m. Earlier de Leeuw et al.[55,56] calculated the surface energy of calcite by subtracting the total energy of a bulk crystal from a total energy of a crystal with an interface while keeping number of particles constant. Using this procedure and the calcite potential model proposed by Pavese et al.,[57] they find values between 590 mN/m[56] and 600 mN/m.[55] Using the same procedure as de Leeuw et al.[55] but with the potential model developed by Rohl et al.,[58] Bruno et al.[59] find a surface energy value of 534 mN/m. Please note that the Pavese et al.[57] and Rohl et al.[58] calcite potentials were tuned to reproduce the equilibrium structure and physical properties such as the elastic constant of calcite. The good agreement of our value with results based on these other potentials is thus very encouraging.

Obtaining the surface energy experimentally is also challenging. Using a double torsion method, Røyne et al.[60] report a value of 320 mN/m for the dry [$10\bar{1}4$] surface. Using electron density functional calculations and the above mentioned subtraction procedure, Kerisit et al.[61] report a surface energy around 426 mN/m. These values are somewhat lower than the majority of classical simulation results on bare calcite, suggesting possible forcefield limitations in describing calcite. (But it is imperative to acknowledge that the experimental and electron density functional results are also not free of assumptions.) However, in assessing the superficial tension (Eq. 2) of a liquid against the mineral and in assessing the contact

angle (Eq. 3), we expect the role of any forcefield limitations to be tempered.

Given the encouraging results for bare calcite, we next consider oil or water against calcite. For oil against calcite, we find $\sigma_{so} = 560$ mN/m, and for water against calcite, we find $\sigma_{sw} = 528$ mN/m. It is clear from these values that, $\zeta_{sw} = 528 - 579 = -51$ mN/m versus $\zeta_{so} = 560 - 579 = -19$ mN/m. Thus both oil and water will wet the bare calcite surface, except that the interaction of water with calcite is predicted to be much stronger. This is expected, since relative to oil, water will interact more strongly with the polar groups on the surface of calcite.

Fig. 2 shows the superficial tension of brine against calcite as a function of ionic strength. We find that as ionic strength is increased, brine will better wet the calcite surface.
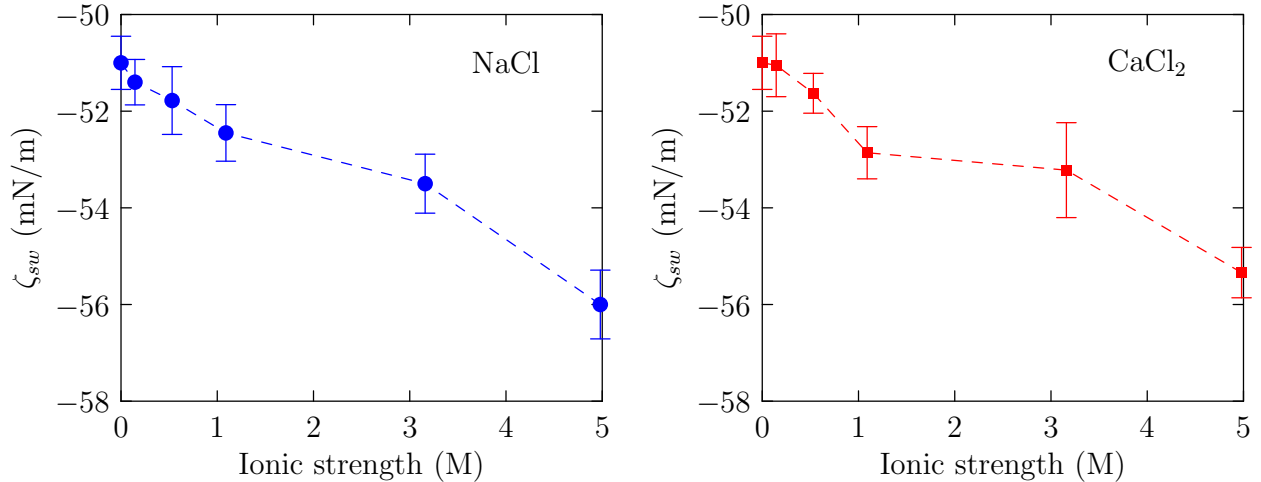

Figure 2: Superficial tension (mN/m) of brine against calcite for different ionic strengths. The error bars represent the 1σ standard deviation from multiple simulations.

Fig. 3 shows the oil/water interfacial tension and $\zeta_{so} - \zeta_{sw}$ with respect to ionic strength for each salt type. For both salts, the oil/water interfacial tension increases with ionic strength, with the stronger effect for $CaCl_2$ over NaCl evident at higher concentrations. Ignoring the salt-type dependence, the increase of interfacial tension with ionic strength is as expected from standard electrostatic arguments.[62] At the low dilution limit, as expected from Debye-Hückel theory, the identity of the salt does not matter. But because the superficial tension
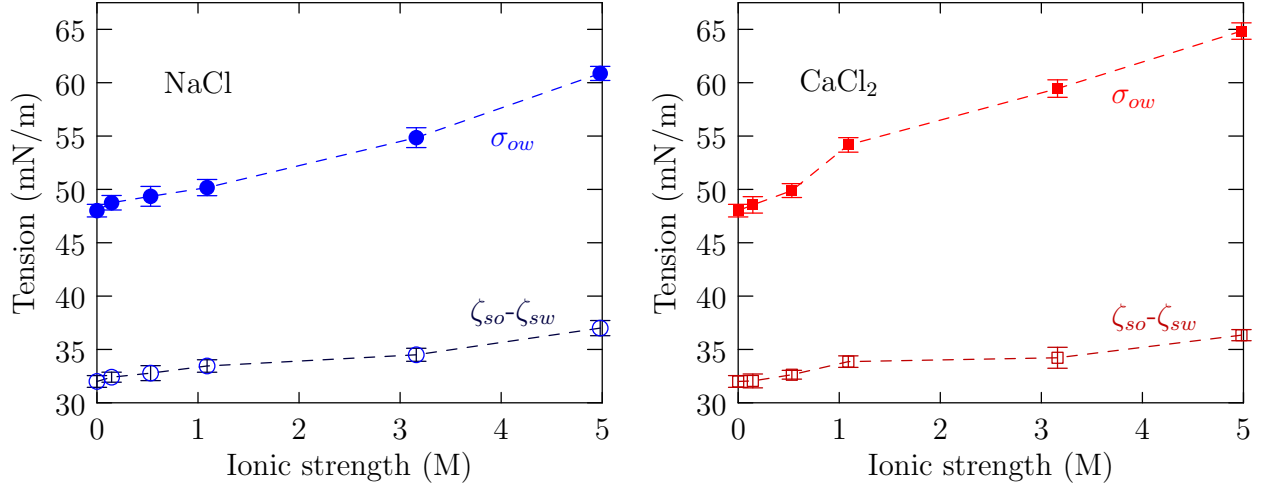
10

Figure 3: Interfacial tension (mN/m) between the model oil and brine at different ionic strengths. Rest as in Figure 2.

of brine against calcite decreases with increasing ionic strength, the factor $\zeta_{so} - \zeta_{sw}$ also increases with increasing ionic strength. But relative to $\zeta_{so} - \zeta_{sw}$, the oil/water tension increases more with ionic strength. The consequence of this feature is that the ratio of $(\zeta_{so} - \zeta_{sw})/\sigma_{ow}$, which is just $\cos(\theta)$ (Eq. 3), decreases with increasing ionic strength (Fig. 4).
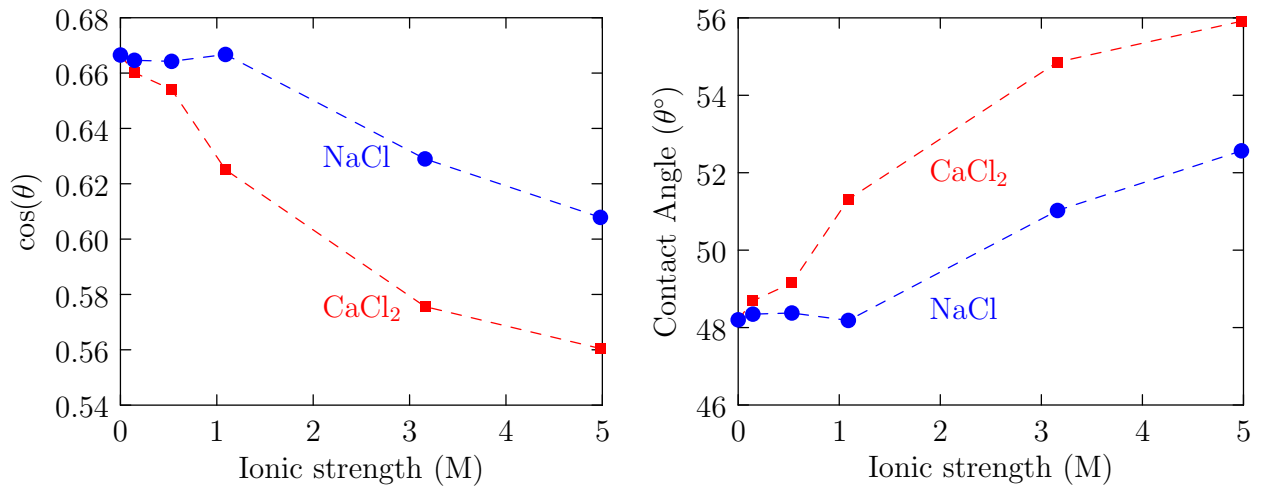

Figure 4: Contact angles obtained using Eq. 3 for brine at different ionic strengths. Notice that in the presence of oil, NaCl is more effective in promoting the wetting of calcite by water than $CaCl_2$.

The observed decrease in the brine/calcite contact angle (in the presence of oil, Fig. ??)

11

with decreasing ionic strength shown in Fig. 4 is consistent with the well-accepted concept of low salinity flooding. In particular, the results show that $CaCl_2$ has a stronger effect on driving the system toward the less water-wet scenario.

Our calculations serve to set a baseline for studies aimed at understanding low-salinity flooding. Importantly, our studies show that while low salinity can disfavor the spreading of brine on calcite, the stabilization of the oil-brine interface can still lead to an overall increase in the wettability of calcite by brine in the presence of oil. Thus our work brings to fore the need to consider the oil-brine interface in discussions of low salinity flooding.

However, it is also important to acknowledge the many challenges in describing systems that are better mimics of actual reservoir conditions. We consider the oil/brine and brine/calcite interfaces in turn.

Our calculations on the oil/brine interfacial tension agree with those of Elena et al.,[63] who used molecular dynamics simulations to investigate the effects of NaCl and $CaCl_2$ on the interfacial tension between brine and pure hydrocarbons (n-dodecane, octane, benzene, and toluene) and hydrocarbon mixtures. However, our results are inconsistent with the experimental results reported by Abdel-Wali et al.[64] and Moiene et al.[65] These authors studied the effect of NaCl and $CaCl_2$ in contact with heavy crude oil, observing an initial decrease followed by an increase in interfacial tension as brine concentration increases, indicating that there may be an optimum brine concentration (20,000 to 40,000 ppm) for reducing the interfacial tension. This effect is likely due to the presence of surface active components in crude oil, which may lead to a non-monotonic behavior of the interfacial tension with respect to ionic strength.[66] Thus while the simple model of oil used here is an important baseline, care should be used in interpreting experimental results based on complex crude oils. Conversely, in experimental studies of low salinity flooding on complex mixtures such as crude oils, much care should be exercised in adapting intuitions based on simple mixtures.

Next consider the brine/calcite interface. It is well appreciated that Ca^{2+} has a strong effect on wettability; for example, see refs.[67,68] Our results (Fig. 4) also show a strong

effect of Ca^{2+} relative to Na^+, but contrary to experimental studies,[67,68] our simulations show that Ca^{2+} should weaken the wettability of calcite by water. This apparent difference arises because of the focus on individual ions, Ca^{2+} versus Na^+. However, in experiments, one has to also contend with the presence of SO_4^{2-}. Thus our work shows that in "smart water" flooding, the anions will also likely play an important role. The simulation techniques developed in this work can prove useful in such investigations, but these are necessarily left to the future.

Conclusions

Most studies on low salinity water flooding agree that the injection of water with a lower ionic strength, compared to that in the reservoir, alters the wettability of the reservoir surface from being less water-wet to more water-wet, which subsequently enhances oil recovery. Our analysis shows that a decrease in ionic strength disfavors the wetting of calcite by water, which is counter to what might be expected based on water adsorbing on to calcite and displacing the oil under low salinity conditions. However, the resolution of this contradiction rests in understanding how ionic strength changes the interfacial properties of the oil-brine system. With decreasing ionic strength, the formation of the oil-brine interface is promoted. On balance, in the oil-brine-calcite system, it is this feature the one that promotes the weakening of adhesion between oil and calcite. Our work brings to fore the need to also consider the oil-brine interface in discussions of low salinity flooding.

Acknowledgement

References

(1) Kokal, S.; Al-Kaabi, A. Enhanced Oil Recovery: Challenges & Opportunities. *World Petroleum Council: Official Publication* **2010**, *64*.

(2) Sheng, J. *Enhanced Oil Recovery Field Case Studies*; Gulf Professional Publishing, 2013.

(3) G, B. G.; West, R. C.; Andresen, K. H. Water Flooding Secondary Recovery Method. 1956; US Patent 2,731,414.

(4) Al-Hadhrami, H. S.; Blunt, M. J. Thermally Induced Wettability Alteration to Improve Oil Recovery in Fractured Reservoirs. SPE/DOE Improved Oil Recovery Symposium. 2000.

(5) Mandal, A. Chemical Flood Enhanced Oil Recovery: A Review. *Intl. J. Oil Gas Coal Techol.* **2015**, *9*, 241–264.

(6) Kantzas, A.; Chatzis, I.; Dullien, F. A. L. Enhanced Oil Recovery by Inert Gas Injection. SPE Enhanced Oil Recovery Symposium. 1988.

(7) Lager, A.; Webb, K. J.; Collins, I. R.; Richmond, D. M. LoSal Enhanced Oil Recovery: Evidence of Enhanced Oil Recovery at the Reservoir Scale. SPE Symposium On Improved Oil Recovery. 2008.

(8) Leach, R. O.; Wagner, O. R.; Wood, H. W.; Harpke, C. F. A Laboratory and Field Study of Wettability Adjustment in Water Flooding. *J. Petrol. Technol.* **1962**, *14*, 206–212.

(9) Morrow, N. R. Wettability and Its Effect on Oil Recovery. *J. Petrol. Technol.* **1990**, *42*, 1–476.

(10) Jadhunandan, P. P.; Morrow, N. R. Effect of Wettability on Waterflood Recovery for Crude-Oil/Brine/Rock Systems. *SPE Res. Eng.* **1995**, *10*, 40–46.

(11) Yildiz, H. O.; Morrow, N. R. Effect of Brine Composition on Recovery of Moutray Crude Oil by Waterflooding. *J. Petrol. Sc. Eng.* **1996**, *14*, 159–168.

(12) Yousef, A. A.; Liu, J. S.; Blanchard, G. W.; Al-Saleh, S.; Al-Zahrani, T.; Al-Zahrani, R. M.; Al-Tammar, H. I.; Al-Mulhim, N. Smart Waterflooding: Industry. SPE Annual Technical Conference and Exhibition. 2012.

(13) Katende, A.; Sagala, F. A Critical Review of Low Salinity Water Flooding: Mechanism, Laboratory and Field Application. *J. Molec. Liq.* **2019**,

(14) Bartels, W.-B.; Mahani, H.; Berg, S.; Hassanizadeh, S. M. Literature Review of Low Salinity Waterflooding from a Length and Time Scale Perspective. *Fuel* **2019**, *236*, 338–353.

(15) Lashkarbolooki, M.; Riazi, M.; Hajibagheri, F.; Ayatollahi, S. Low salinity injection into asphaltenic-carbonate oil reservoir, mechanistical study. *J. Molec. Liq.* **2016**, *216*, 377–386.

(16) Wei, B.; Lu, L.; Li, Q.; Li, H.; Ning, X. Mechanistic Study of Oil/Brine/Solid Interfacial Behaviors During Low-Salinity Waterflooding Using Visual and Quantitative Methods. *Energy Fuels* **2017**, *31*, 6615–6624.

(17) Green, D. W.; Willhite, G. P. Enhanced Oil Recovery, SPE Textbook Series. *Society of Petroleum Engineers, Richardson, Texas* **1998**,

(18) Zolotukhin, A. B.; Ursin, J. R. *Introduction to Petroleum Reservoir Engineering*; Norwegien Academic Press (HóyskoleForlaget), 2000.

(19) Bikerman, J. J. *Inorganic and Physical Chemistry*; Springer, 1978; pp 1–66.

(20) Makkonen, L. Young's Equation Revisited. *J. Phys. Cond. Matt.* **2016**, *28*, 135001.

(21) Douillard, J. M.; Zoungrana, T.; Partyka, S. Surface Gibbs Free Energy of Minerals: Some Values. *J. Petrol. Sc. Eng.* **1995**, *14*, 51–57.

(22) Gibbs, J. W. *The scientific papers of J. Willard Gibbs*; Ox Bow Press, 1993; Vol. 1; Chapter 3: Equilibrium of heterogeneous substances — Surfaces of Discontinuity Between Solids and Fluids, pp 314–331.

(23) Johnson, Jr., R. E. Conflicts Between Gibbsian Thermodynamics and Recent Treatments of Interfacial Energies in Solid-Liquid-Vapor Systems. *J. Phys. Chem.* **1959**, *63*, 1655–1658.

(24) Gloor, G. J.; Jackson, G.; Blas, F. J.; de Miguel, E. Test-Area Simulation Method for the Direct Determination of the Interfacial Tension of Systems with Continuous or Discontinuous Potentials. *J. Chem. Phys.* **2005**, *123*, 134703.

(25) Vega, C.; de Miguel, E. Surface Tension of the Most Popular Models of Water by Using The Test-Area Simulation Method. *J. Chem. Phys.* **2007**, *126*, 154707.

(26) Ghoufi, A.; Goujon, F.; Lachet, V.; Malfreyt, P. Surface Tension of Water and Acid Gases from Monte Carlo Simulations. *J. Chem. Phys.* **2008**, *128*, 154716.

(27) Bahadur, R.; Russell, L. M.; Alavi, S. Surface Tensions in NaCl-Water-Air Systems from MD Simulations. *J. Phys. Chem. B* **2007**, *111*, 11989–11996.

(28) Nair, A. R.; Sathian, S. P. A Molecular Dynamics Study to Determine the Solid-Liquid Interfacial Tension Using Test Area Simulation Method (TASM). *J. Chem. Phys.* **2012**, *137*, 084702.

(29) Errington, J. R.; Kofke, D. A. Calculation of Surface Tension Via Area Sampling. *J. Chem. Phys.* **2007**, *127*, 174709.

(30) Lu, N.; Kofke, D. A. Accuracy of free-energy perturbation calculations in molecular simulations. I. Modeling. *J. Chem. Phys.* **2001**, *114*, 7303–7311.

(31) Pohorille, A.; Jarzynski, C.; Chipot, C. Good Practice in Free-Energy Calculations. *J. Phys. Chem. B* **2010**, *114*, 10235–10253.

(32) Salomons, E.; Mareschal, M. Surface Tension, Adsorption and Surface Entropy of Liquid-Vapour Systems by Atomistic Simulation. *J. Phys. Cond. Matt.* **1991**, *3*, 3645.

(33) Guo, W.; Errington, J. R. Monte Carlo Simulation Strategies to Compute the Interfacial Properties of a Model Octane-Water-Silica System. *J. Phys. Chem. C* **2018**, *122*, 17309–17318.

(34) Leroy, F.; Müller-Plathe, F. Solid-Liquid Surface Free Energy of Lennard-Jones Liquid on Smooth and Rough Surfaces Computed by Molecular Dynamics Using the Phantom-Wall Method. *J. Chem. Phys.* **2010**, *133*, 044110.

(35) Qi, X.; Zhou, Y.; Fichthorn, K. A. Obtaining the Solid-Liquid Interfacial Free Energy Via Multi-Scheme Thermodynamic Integration: Ag-Ethylene Glycol Interfaces. *J. Chem. Phys.* **2016**, *145*, 194108.

(36) Jiang, H.; Müller-Plathe, F.; Panagiotopoulos, A. Z. Contact Angles From Young's Equation in Molecular Dynamics Simulations. *J. Chem. Phys.* **2017**, *147*, 084708.

(37) France-Lanord, A.; Rigby, D.; Mavromaras, A.; Eyert, V.; Saxe, P.; Freeman, C.; Wimmer, E. MedeA®: Atomistic Simulations for Designing and Testing Materials for Micro/Nano Electronics Systems. 2014; DOI:10.1109/eurosime.2014.6813850.

(38) Yiannourakou, M.; Ungerer, P.; Leblanc, B.; Rozanska, X.; Saxe, P.; Vidal-Gilbert, S.; Gouth, F.; Montel, F. Molecular Simulation of Adsorption in Microporous Materials. *Oil Gas Sci. Technol.– Rev. IFP Energies nouvelles* **2013**, *68*, 977–994.

(39) Sun, H.; Mumby, S. J.; Maple, J. R.; Hagler, A. T. An Ab Initio CFF93 All-Atom Force Field for Polycarbonates. *J. Am. Chem. Soc.* **1994**, *116*, 2978–2987.

(40) Waldman, M.; Hagler, A. T. New Combining Rules for Rare Gas Van der Waals Parameters. *J. Comp. Chem.* **1993**, *14*, 1077–1084.

(41) de Leeuw, N. H.; Parker, S. C. Surface Structure and Morphology of Calcium Carbonate Polymorphs Calcite, Aragonite, and Vaterite: An Atomistic Approach. *J. Phys. Chem. B* **1998**, *102*, 2914–2922.

(42) de Leeuw, N. H. Surface Structures, Stabilities, and Growth of Magnesian Calcites: A Computational Investigation From The Perspective of Dolomite Formation. *Am. Mineralogist* **2002**, *87*, 679–689.

(43) Titiloye, J. O.; De Leeuw, N. H.; Parker, S. C. Atomistic Simulation of the Differences Between Calcite and Dolomite Surfaces. *Geochim. Cosmochim. Acta* **1998**, *62*, 2637–2641.

(44) Koleini, M. M.; Mehraban, M. F.; Ayatollahi, S. Effects of Low Salinity Water on Calcite/Brine Interface: A Molecular Dynamics Simulation Study. *Coll. Surf. A* **2018**, *537*, 61–68.

(45) Koleini, M. M.; Badizad, M. H.; Kargozarfard, Z.; Ayatollahi, S. Interactions Between Rock/Brine and Oil/Brine Interfaces Within Thin Brine Film Wetting Carbonates: A Molecular Dynamics Simulation Study. *Energy Fuels* **2019**,

(46) Sedghi, M.; Piri, M.; Goual, L. Atomistic Molecular Dynamics Simulations of Crude Oil/Brine Displacement in Calcite Mesopores. *Langmuir* **2016**, *32*, 3375–3384.

(47) Shen, J.-W.; Li, C.; van der Vegt, N. F. A.; Peter, C. Understanding the Control of Mineralization by Polyelectrolyte Additives: Simulation of Preferential Binding to Calcite Surfaces. *J. Phys. Chem. C* **2013**, *117*, 6904–6913.

(48) Plimpton, S. Fast Parallel Algorithms for Short-Range Molecular Dynamics. *J. Comp. Phys.* **1995**, *117*, 1–19.

(49) LAMMPS. Sandia National Laboratories, 2019; http://lammps.sandia.gov.

(50) Hoover, W. G. Canonical Dnamics: Equilibrium Phase-Space Distributions. *Phys. Rev. A* **1985**, *31*, 1695.

(51) Hoover, W. G. Constant-Pressure Equations of Motion. *Phys. Rev. A* **1986**, *34*, 2499.

(52) Richards, T. W.; Coombs, L. The Surface Tensions of Water, Methyl, Ethyl and Butyl Alcohols, Ethyl Butyrate, Benzene and Toluene. *J. Am. Chem. Soc.* **1915**, *37*, 1656–1676.

(53) Richards, T. W.; Carver, E. K. A Critical Study of the Capillary Rise Method of Determining Surface Tension, with Data for Water, Benzene, Toluene, Chloroform, Carbon Tetrachloride, Ether and Dimethyl Aniline. *J. Am. Chem. Soc.* **1921**, *43*, 827–847.

(54) Vargaftik, N. B.; Volkov, B. N.; Voljak, L. D. International Tables of the Surface Tension of Water. *J. Phys. Chem. Ref. Data* **1983**, *12*, 817–820.

(55) de Leeuw, N. H.; Parker, S. C. Atomistic Simulation of the Effect of Molecular Adsorption of Water on the Surface Structure and Energies of Calcite Surfaces. *J. Chem. Soc. Faraday Trans.* **1997**, *93*, 467–475.

(56) de Leeuw, N. H.; Parker, S. C.; Rao, K. H. Modeling the Competitive Adsorption of Water and Methanoic Acid on Calcite and Fluorite Surfaces. *Langmuir* **1998**, *14*, 5900–5906.

(57) Pavese, A.; Catti, M.; Parker, S. C.; Wall, A. Modelling of the Thermal Dependence of Structural and Elastic Properties of Calcite, $CaCO_3$. *Phys. Chem. Minerals* **1996**, *23*, 1–5.

(58) Rohl, A. L.; Wright, K.; Gale, J. D. Evidence From Surface Phonons for the (2x1) Reconstruction of the $(10\bar{1}4)$ Surface of Calcite From Computer Simulation. *Am. Mineral* **2003**, *88*, 921–925.

(59) Bruno, M.; Massaro, F. R.; Pastero, L.; Costa, E.; Rubbo, M.; Prencipe, M.; Aquilano, D. New Estimates of the Free Energy of Calcite/Water Interfaces for Evaluating the Equilibrium Shape and Nucleation Mechanisms. *Cryst. Growth Des.* **2013**, *13*, 1170–1179.

(60) Røyne, A.; Bisschop, J.; Dysthe, D. K. Experimental Investigation of Surface Energy and Subcritical Crack Growth in Calcite. *J. Geophys. Res.* **2011**, *116*, 19–10.

(61) Kerisit, S.; Parker, S. C.; Harding, J. H. Atomistic Simulation of the Dissociative Adsorption of Water on Calcite Surfaces. *J. Phys. Chem. B* **2003**, *107*, 7676–7682.

(62) Onsager, L.; Samaras, N. N. T. The Surface Tension of Debye-Hückel Electrolytes. *J. Chem. Phys.* **1934**, *2*, 528–536.

(63) Rodríguez Remesal, E.; Amaya Suárez, J.; Márquez Cruz, A. M.; Fernández Sanz, J.; Rincón, C.; Guitián, J. Molecular Dynamics Simulations of the Role of Salinity and Temperature on the Hydrocarbon/Water Interfacial Tension. *Theo. Chem. Acc.* **2017**,

(64) Abdel-Wali, A. A. Effect of Simple Polar Compounds and Salinity on Interfacial Tension and Wettability of Rock/Oil/Brine System. *J. King Saud Univ. Eng. Sc.* **1996**, *8*, 153–162.

(65) Moeini, F.; Hemmati-Sarapardeh, A.; Ghazanfari, M.-H.; Masihi, M.; Ayatollahi, S. Toward Mechanistic Understanding of Heavy Crude Oil/Brine Interfacial Tension: The Roles of Salinity, Temperature and Pressure. *Fluid Phase Eql.* **2014**, *375*, 191–200.

(66) Chávez-Miyauchi, T. E.; Firoozabadi, A.; Fuller, G. G. Nonmonotonic Elasticity of the Crude Oil-Brine Interface in Relation to Improved Oil Recovery. *Langmuir* **2016**, *32*, 2192–2198.

(67) Strand, S.; Høgnesen, E. J.; Austad, T. Wettability Alteration of Carbonates — Effects

of Potential Determining Ions (Ca^{2+} and SO_4^{2-}) and Temperature. *Coll. Surf. A* **2006**, *275*, 1–10.

(68) Song, J.; Wang, Q.; Shaik, I.; Puerto, M.; Bikkina, P.; Aichele, C.; Biswal, S. L.; Hirasaki, G. J. Effect of Salinity, Mg^{2+} and $SO_4^{2}-$ on "Smart Water"-Induced Carbonate Wettability Alteration in a Model Oil System. *J. Coll. Int. Sc.* **2020**, *563*, 145–155.

Graphical TOC Entry